Environmental Science Processes & Impacts

ROYAL SOCIETY OF CHEMISTRY

PAPER

View Article Online
View Journal | View Issue

Cite this: *Environ. Sci.: Processes Impacts*, 2025, **27**, 2422

Decay rate of gas-phase peracetic acid in a polyvinyl fluoride sample bag†

Amos Doepke, * Robert P. Streicher and Angela L. Stastny

In this study the temperature dependent decay rate of gas-phase peracetic acid (PAA) concentrations in polyvinyl fluoride (PVF) sample bags was measured. Headspace from a PAA solution was used to dynamically generate atmospheres of gas-phase PAA which were transferred to PVF bags. The concentration of gas-phase PAA in PVF bags, in a temperature-controlled environment, was measured *versus* time using both selected ion flow-tube mass spectrometry (SIFT-MS) and impinger based colorimetric measurements. A review of PAA decomposition reactions, kinetics, and results of SIFT-MS measure of PAA and acetic acid are discussed. Gas-phase PAA concentrations in the PVF bags exhibited exponential decay consistent with first-order kinetics. The temperature dependent decay rate of gas-phase PAA concentration in PVF sample bags had half-lives that ranged from 19 h (at 30 °C) to 45 h (at 10 °C). From the Arrhenius equation, an activation energy of 34.2 ± 1.1 kJ mol^{-1} (8.2 ± 0.3 kcal mol^{-1}) was calculated from the temperature dependence of the decay constant. In this work, the half-lives of gas-phase PAA concentrations measured in PVF were considerably longer than other studies of PAA in containers.

Received 14th April 2025
Accepted 16th June 2025

DOI: 10.1039/d5em00286a

rsc.li/espi

Environmental significance

Peracetic acid (PAA) is the second most abundant organic peroxide in the troposphere and the third most abundant in urban air. Understanding the gas-phase half-life of PAA is crucial for modeling its atmospheric chemistry, environmental cycling, and assessing industrial processes and occupational safety. However, data on the gas-phase decay kinetics of PAA are limited. This manuscript provides new insights into the fate of PAA by measuring temperature-dependent decay rates and kinetics, which may be applicable in both natural and engineered systems. Our findings indicate that the half-lives of gas-phase PAA were significantly longer than those reported in other studies, emphasizing the need for further investigation into PAA behavior in various environmental contexts.

Introduction

The half-life of peracetic acid (PAA) in the gas-phase is important for modeling atmospheric chemistry[1–5] and environmental cycling of PAA,[4,6–8] evaluating industrial processes[9] and occupational safety.[10,11] Significant anthropogenic generation and release of gas-phase PAA occurs in occupational settings *via* biomass burning, material processing (bleaching),[12] and disinfection.[11,13,14]

PAA has been replacing chlorinated chemicals in many processes because it has been regarded as less harmful to the environment, due to producing fewer hazardous disinfection byproducts compared to chlorinated disinfectants;.[15,16] The steady increase in PAA production and use in industrial settings is expected to increase occupational exposure to PAA.[17] PAA is a strong oxidant that can cause chemical burns, irritation to eyes, and the upper respiratory system.[18] Measuring PAA concentrations in occupational settings and evaluating the relationship between worker exposure to PAA and the effects on worker health are areas of recent research.[11,19,20] To address concerns about occupational exposure, the American Conference of Governmental Industrial Hygienists (ACGIH) set a Threshold Limit Value (TLV) for short-term exposure limit (STEL) of 0.4 ppm for an inhalable fraction and vapor in 2014.[21]

PAA is relatively volatile with a vapor pressure of 14.5 mm Hg at 25 °C,[22] and readily enters the air through evaporation from PAA solutions. The application of PAA by wiping or spraying solutions allows gas-phase PAA and/or aerosols to expose workers which has been documented in surface disinfection processes[19,23,24] and meat processing.[25,26] Environmental controls such as isolation and ventilation have typically been used to reduce PAA exposure.[27] However, in occupational environments, a significant concentration of PAA applied as a surface disinfectant ends up in the gas phase.[23,28,29]

The primary goal of the studies herein was measuring the change in gas-phase PAA concentrations in a PVF sampling bag to calculate a half-life and activation energy (E_a) of the decay of gas-phase PAA. It was known that gas-phase PAA has a limited lifetime due to energetic decomposition and surface

National Institute for Occupational Safety and Health, Health Effects Laboratory Division, Cincinnati, Ohio 45226, USA. E-mail: adoepke@cdc.gov

† Electronic supplementary information (ESI) available. See DOI: https://doi.org/10.1039/d5em00286a

interactions.[8] PVF bags were chosen for their ability to isolate samples of gas-phase PAA and were considered inert or resistant to attacks by many chemicals.[30] It was proposed that measurements of PAA concentration decay in a PVF bag would primarily represent gas phase processes and minimize surface reactivity. We anticipated being able to apply what was learned by measuring the half-life of gas-phase PAA to residence time of PAA in occupational environments. These experiments could provide information about the use of PVF bags for sampling of PAA for occupational exposures.[31,32] Measurements of occupationally relevant decomposition or decay of gas-phase PAA have been addressed in relatively few publications. In addition to the studies herein, the authors present a discussion of relevant PAA decomposition reactions and kinetics of PAA.

PAA decomposition routes and kinetics

Peracetic acid decomposition has been generalized *via* three reaction pathways: hydrolysis, catalyzed decomposition, and spontaneous decomposition. Reaction (1), represents the decomposition of PAA to acetic acid (AA) and hydrogen peroxide (HP) through hydrolysis, followed by the spontaneous decomposition of HP in reaction (2).[33]

$$CH_3COOOH + H_2O \rightarrow CH_3COOH + H_2O_2 \quad (1)$$

$$2H_2O_2 \rightarrow 2H_2O + O_2 \quad (2)$$

Reaction (3) has been described as a surface mediated decomposition[34] and a spontaneous decomposition,[35] that yields AA and O_2 as products. The reaction mechanism for spontaneous decomposition in liquid has been proposed as a peracetic anion nucleophilic attack on the carbonyl carbon of a second PAA molecule in neutral or alkaline conditions.[9,36] While in acidic conditions, been proposed that decomposition proceeds through protonation of an oxygen in PAA (most likely on the carbonyl oxygen). The protonated PAA interacts with a second PAA molecule to form an unstable intermediate that decomposes to O_2 and AA.[35]

$$2CH_3COOOH \rightarrow 2CH_3COOH + O_2 \quad (3)$$

Transition metal catalyzed decomposition of PAA, in reaction (4), releases significant amounts of oxygen and heat which can lead to runaway reactions.[37]

$$CH_3COOOH \xrightarrow{M^{n+}} O_2 + \text{other decomposition products} \quad (4)$$

Mechanical shock, heat, and light can be initiators of homolytic cleavage of the O–O bond where two products, acetyloxy and hydroxyl radicals are generated as in reaction (5).[37,38] Secondary reactions (6) and (7) produce reaction products including CO_2, methane, ethane and additional compounds.[37]

$$CH_3COOOH \rightarrow CH_3COO\cdot + \cdot OH \quad (5)$$

$$CH_3COO\cdot \rightarrow CH_3^{\cdot} + CO_2 \quad (6)$$

$$CH_3^{\cdot} + CH_3COOH \rightarrow CH_3OH + CH_3COO\cdot \quad (7)$$

Oxidation of PAA through an addition of ·OH in a pre-reactive complex has been shown to be a favored reaction mechanism in atmospheric chemistry. The oxidation of PAA is considered to primarily occur through two pathways: the abstraction of acidic hydrogen and the abstraction of a methyl hydrogen, with both generating formaldehyde as the principal reaction product.[3] Additionally, radical reactions of HO_x are important in the PAA degradation pathway.[39] However, this process is often presented as a simplified pathway in reaction (8).

$$CH_3COOOH \rightarrow CH_3OH + CO_2 \quad (8)$$

Liquid-phase kinetics of PAA decomposition were reported in multiple publications. Musakka *et al.* observed zero order, first order, as well as complex kinetics involved in the liquid-phase decomposition of PAA.[33] While the liquid-phase spontaneous decomposition in reaction (3) has been described as a second-order reaction with respect to PAA concentration.[35]

The overall rate of gas phase decomposition of PAA has been shown to follow first order kinetics.[34,39,40] The observed pseudo first-order rate constant k_0 has been described by Schmidt and Sehon as a combination of the two reactions (3) and (5) as shown in eqn (9).[34]

$$-\frac{d[PAA]}{dt} = k_0[PAA] = (k_3 + k_5)[PAA] \quad (9)$$

where k_3 and k_5 represent the rate constants for reactions (3) and (5), respectively.

In gas-phase pyrolytic decomposition experiments, Schmidt and Sehon showed that changing the surface area inside the reaction vessel could affect the ratio of AA to CO_2, with increased surface area resulting in a larger ratio.[34] Increased surface area presumably shifted the decomposition away from an energetically initiated decomposition as in eqn (5) and (6) to a surface mediated pathway as in reaction eqn (3). Schmidt and Sehon used toluene as a carrier, which was expected to eliminate the hydrolytic decomposition in favor of O–O bond cleavage.[34,41]

There have been two measurements of the decay of gas-phase PAA at ambient temperatures to determine a half-life which were relevant to the work herein. In an unpublished report, Ancker and Zetterberg (reported in ref. 42) determined a 22 minutes half-life for gas-phase PAA measured *via* long-path Fourier transform infrared spectroscopy in a sail-cloth bag.[42–44] While Hines *et al.* found a gas-phase PAA half-life of 83 minutes in a small (0.16 m^3) chamber containing a recirculating fan.[29] Neither of these studied the temperature dependence of PAA decay.

Arrhenius equation

The Arrhenius equation describes the temperature dependence of chemical reaction rates. A rearrangement of the Arrhenius equation yields eqn (10), which has the form of a line as ($y = mx + b$).

$$\ln k = \frac{-E_a}{R}\left(\frac{1}{T}\right) + \ln A \quad (10)$$

where k is the rate constant (s^{-1}) for the reaction, T is the temperature in Kelvin, A is the pre-exponential factor, E_a is the molar activation energy for the reaction, and R is the universal gas constant (J K^{-1} mol^{-1}). The E_a for a thermal reaction rate constant $k(T)$, can be defined as $(-R)$ times the slope of the plot of $\ln k$ *vs.* $(1/T)$, known as the Arrhenius plot, as in eqn (11).

$$E_a \underset{=}{\text{def}} - R\left[\frac{\partial \ln k}{\partial(1/T)}\right] \quad (11)$$

There have been relatively few gas phase experiments elucidating an E_a of PAA. The E_a is the minimum energy requirement or energy barrier to initiate a chemical reaction. The value of E_a provides insight into the reaction mechanism(s).[45] The pyrolytic (127–360 °C) decomposition of gas-phase PAA was reported by Schmidt and Sehon to have an E_a of 126 to 142 kJ mol^{-1} (30–34 kcal mol^{-1}) for dissociation of the PAA O–O bond.[34]

Bianchini *et al.* used density functional theory (DFT) to calculate a bond dissociation energy of 159 kJ mol^{-1} (38 kcal mol^{-1}) for the O–OH bond of PAA.[46] The bond energy of PAA is often contrasted with the greater dissociation energy of hydrogen peroxide at 213 kJ mol^{-1} (51 kcal mol^{-1}).[47]

Activation energies of PAA decomposition in water reported by Musakka *et al.* were 65.2 kJ mol^{-1} for reaction (1), 179 kJ mol^{-1} for reaction (2), and 154 kJ mol^{-1} for a reaction pathway as described by reaction (8). In bleach solutions at pH 7.1, an E_a of 99.6 kJ mol^{-1} (23.8 kcal mol^{-1}) was reported by Rucker and Cates.[48] Kunigk *et al.* reported that aqueous PAA decomposition followed first order reaction kinetics with an E_a of 60 kJ mol^{-1} observed for hydrolysis.[40] Wang *et al.* observed an E_a of 49.8 kJ mol^{-1} in a pH 7 phosphate buffer solution. Experimentally derived activation energies can represent an ensemble of reaction pathways unless specific measures are taken to force reactions *via* a singular mechanism.

Materials and methods

A dynamic atmosphere generation-system, as previously described in Doepke *et al.*, was used to generate atmospheres at controlled temperatures (10 to 30 °C), humidities and concentrations of gas-phase PAA.[52] Headspace from 32% PAA solution (Sigma-Aldrich, St. Louis, MO) was used as the gas-phase PAA source. A continuous flow of air over the headspace of a vial containing PAA solution was mixed with humidity- and temperature-conditioned air to produce final concentrations of gas-phase PAA in a stream of air. The air through the headspace of the PAA vial was controlled with a needle valve which could be adjusted to control the gas-phase PAA concentration. Impinger measurements, which are described below, were used to measure the gas-phase PAA concentrations in the generated air. For the experiments herein, the target concentration of gas-phase PAA in the generated air was 0.4 ppmv. The continuous flow of gas-phase PAA containing air was routed through tubing in a temperature-controlled chamber.

A 100 liter Tedlar® (polyvinyl fluoride, PVF) sample bag (232–100, SKC Inc., Eighty Four, Pennsylvania) with a polypropylene valve was placed in a sealed case (Vac-U-Chamber, SKC-West Inc., Fullerton, CA). Metal fittings in the Vac-U-Chamber were replaced with polypropylene and polytetrafluoroethylene (PTFE) fittings. The PVF bag was connected to the atmosphere generation system *via* PTFE tubing through the SKC case. A tube connected the case to a vacuum line, which created an area of low pressure inside the case, causing gas-phase PAA laden air to be drawn from the generation system into the PVF bag inside the case. The PVF sample bags were filled to approximately two-thirds of their capacity (which took about 5 minutes) with PAA laden air from the dynamic atmosphere generation system. When using a new PVF bag, the decay rate of the PAA concentration was faster for the first few times that the bag was refilled with atmospheres generated from headspace of a PAA solution. The PAA decay-rate stabilized after using the bag for about four refills of gas-phase PAA that were left in the bag overnight. Subsequent experiments were all done using the same bag. The bag was flushed with air three times between experiments.

For kinetics experiments, the filled PVF bag was moved to the temperature controlled environmental chamber where the gas-phase PAA concentration in the bag was measured using an impinger sampling method. Use of an impinger to measure PAA was demonstrated in Stastny *et al.*[20] and briefly described below. The inlet of a 50 mL glass impinger (Ace Glass Inc., Vineland, NJ) was connected to the PVF sample bag *via* Tygon® tubing. The impinger was filled with 15 mL of >18 MΩ-cm deionized water. The impinger outlet was connected to a 1 L min^{-1} flow-limiting critical orifice (Millipore, St. Louis, MO) and then a vacuum pump (MZ 2 NT, Vacuubrand Inc., Essex, CT). Before sampling, a flowmeter (Bios DryCal Defender, Mesa Labs, Lakewood, CO) was used to validate the critical orifice flow rate. The impinger sampled for 15 minutes, passing 15 liters of air through the impinger solution from the PVF bag. A photometer (V-2000, Chemetrics, Midland, VA) and PAA test kits (Vacu-vials K-7913, Chemetrics, Midland, VA) were used to measure the PAA in the impinger solution, which was then converted to a gas-phase PAA concentration in the sampled air.

After measuring the gas-phase PAA concentration *via* impinger, the PVF bag was connected to a SIFT-MS (Voice 2000, Syft Technologies, Christchurch, New Zealand) with an HDI inlet with a flow rate of 20 mL min^{-1}. The SIFT-MS used He as a carrier gas and was operated using positive reagent ions and in selected ion mode with a dwell time of 100 ms per ion. A list of scanned ions and corresponding products is in the ESI in Table S1.† The PVF bag was connected to the SIFT-MS *via* 1/8″ i.d. PTFE tubing. An inline electronically actuated pinch-valve controlled the flow of gas from the bag to the SIFT-MS. A block diagram of the arrangement is provided as Fig. S1 in the ESI.† The pinch valve was controlled by an electronic timer which opened the valve for 10 minutes each hour. The use of the automated valve to interrupt the flow of gas from the bag made it possible to extend SIFT-MS measurements to 48 hours without consuming a large volume of the bag contents. At the end of the 10 minutes sampling period (open pinch valve), the

last 10 data points from the SIFT-MS (counts per second) were averaged for each ion. The SIFT-MS sampling frequency was 0.3 Hz in a selected ion mode with a dwell time of 100 ms per ion. At the end of the experimental time frame (24 or 48 h), a second impinger measurement of gas-phase PAA in the PVF bag was done. Impinger measurements were limited to the beginning and end of the experiment because the impinger used 15 liters per measurement, which consumed a large portion of the total volume of gas in the bag.

Measurements of peracetic acid and acetic acid *via* SIFT-MS

Selected-ion flow-tube mass spectrometry (SIFT-MS) uses plasma to generate ions from air (reagent ions) which are then reacted with gas-phase analyte (to produce analyte ions). Reagent ions used herein were H_3O^+, NO^+ and O_2^+. In general, eqn (12) represents the gas-phase analyte concentration [A] in the flow tube as follows,

$$[A] = \frac{[P^+]ICF_P}{k_r \times t_r \times [R^+]ICF_R} \quad (12)$$

where $[P^+]$ is the product ion counts, $[R^+]$ is the reagent ion counts, ICF_P and ICF_R are instrumental calibration functions for the product ions and reagent ions, respectively, k_r with units of $cm^3\ s^{-1}$ is the reaction rate between the reagent ion and analyte to produce product ions, and t_r is the reaction time, or residence time in the flow tube.[49] The concentration of the reagent ions and their collision rate (k_c) with other molecules in the flow tube are known. For H_3O^+ the k_r is typically equal to the k_c, but for NO^+ and O_2^+, k_r is less than k_c. The collision rates, reaction rates, and product ions for each of the reagent ions H_3O^+, NO^+, and O_2^+ have previously been determined for PAA, AA and H_2O_2 and are listed in Table S2 in the ESI†[50,51] along with a discussion of the product ions observed for PAA and AA.

Results and discussion

Decay of gas-phase PAA in a PVF bag

A plot of the SIFT-MS response as ions associated with PAA (H_3O^+ *m*/*z* 77+) counts per second *versus* the time, during 48 hours, are shown in Fig. 1 fitted with an exponential decay function. The initial and final PAA concentrations in the PVF bag measured *via* impinger were also included in Fig. 1.

The rate of decay of counts of the *m*/*z* 77+ ion aligned with independent impinger measurements of PAA concentrations. SIFT-MS data points in Fig. 1 were the average of the last 10 datapoints collected during the 10 min per hour sampling periods when the SIFT-MS was sampling from the PVF bag. A representative plot of the ions produced by AA (H_3O^+ *m*/*z* 61+) and PAA (H_3O^+ *m*/*z* 77+) during the 10 minutes sampling periods are shown in Fig. S2 of the ESI.† Fig. S2† shows that the AA signal took most of the 10 minutes to reach >90% of its maximum, while the PAA signal stabilized around 5 minutes after the valve opened. Španěl *et al.* estimated that only 10% of the PAA produces H_3O^+ *m*/*z* 77+ in the SIFT-MS, with the remaining 90% of PAA decomposing to AA with a H_3O^+ *m*/*z* 61+.[50] AA has been known to readily adsorb to inlets and transfer lines, often resulting in a negative measurement bias,[53] which may account for some of the long stabilization time for the AA signal in Fig. S2.†

The exponential decay of the gas-phase PAA concentration *via* the counts per second of the *m*/*z* 77+ ion, was consistent with first-order reaction kinetics, which was used to determine a decay rate constant from the fitting of the equation $y = ae^{kx}$, where k was the rate constant. Separately, a half-life and decay constant were determined *via* the initial and final impinger measurements of PAA concentration.

In previous work, by Doepke *et al.*, evaluation of the relative abundance of PAA, AA and H_2O_2 from headspace of a 32% PAA

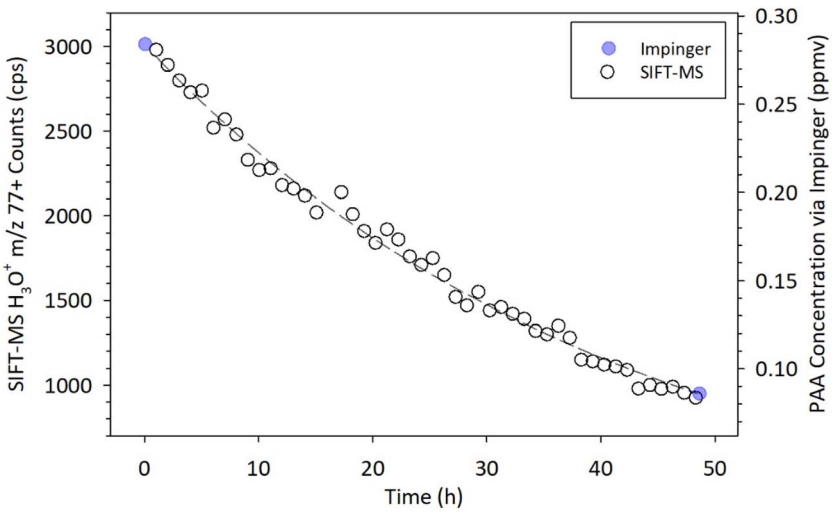

Fig. 1 Concentration decay of gas-phase PAA in a PVF sample bag using *m*/*z* 77+ ion counts from SIFT-MS (open circle) *versus* time fit to an exponential decay curve (dashed line) and impinger measurements (shown by filled blue circle) done at the beginning and end of the measurement time frame.

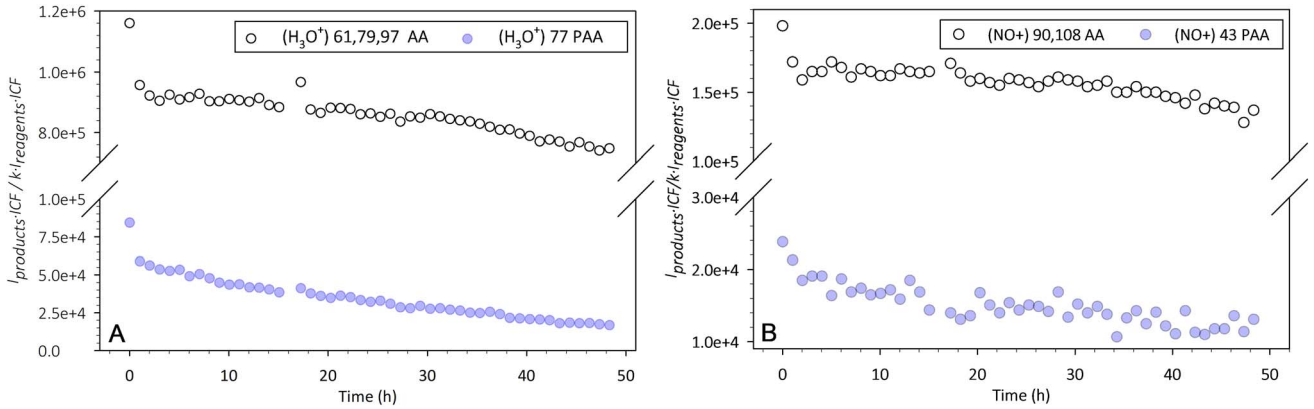

Fig. 2 (A) and (B) Representative responses of acetic acid and peracetic acid *versus* time as determined by product ion counts of the H_3O^+ reagent ion (A) and NO^+ reagent ion (B).

solution showed that there was a relatively large concentration of gas-phase AA in the headspace which became part of the atmospheres generated in this type of system.[52] In addition to the initial concentration of AA, an increase in the concentration of AA should be observable at the same rate as the decay of PAA such that $\Delta[AA] = -\Delta[PAA]$ *via* reactions (1) or (3). However, the response for both PAA and AA decreased with time as shown in Fig. 2A and B. Table S2 (in the ESI)† lists reagent ions and production ions for AA and PAA. In our observations, the H_3O^+ reagent ion and the product ion m/z 77+ had the highest sensitivity to PAA compared to the NO + m/z 43+ product (both are reagent-product ion combinations that can be uniquely attributed to PAA) as seen in the difference in response from PAA in Fig. 2A and B. The change in response between the initial data point and the second data point in both Fig. 2A and B, are interpreted as establishing a surface adsorption equilibrium in the PVF bag, resulting in a decrease of the gas-phase concentration of both PAA and AA. The concentration of PAA measured by impinger in the PVF bag (~0.3 ppmv in Fig. 1) was always less than the concentration measured in the atmosphere generation system (~0.4 ppmv) prior to filling to the PVF bag. The initial SIFT-MS datapoint was not included in determinations of the rate constant (*via* fitting of the exponential curve) from the SIFT-MS data.

In Fig. 2A and B the response from or decrease in AA was thought to be offset by the generation of AA *via* PAA decomposition. The sustained loss of AA over the time frame we observed was consistent with other reports. While there are several pathways for AA decomposition in gas phase and at surfaces, there is no evidence that the conditions for AA decomposition are present in PVF sample bags.[54] In a study of exhaled breath constituents in PVF sample bags, Fido *et al.* showed that AA decreased to less than 30% of the initial concentration after 48 h.[55] Similarly, Kasper *et al.* showed that AA followed an

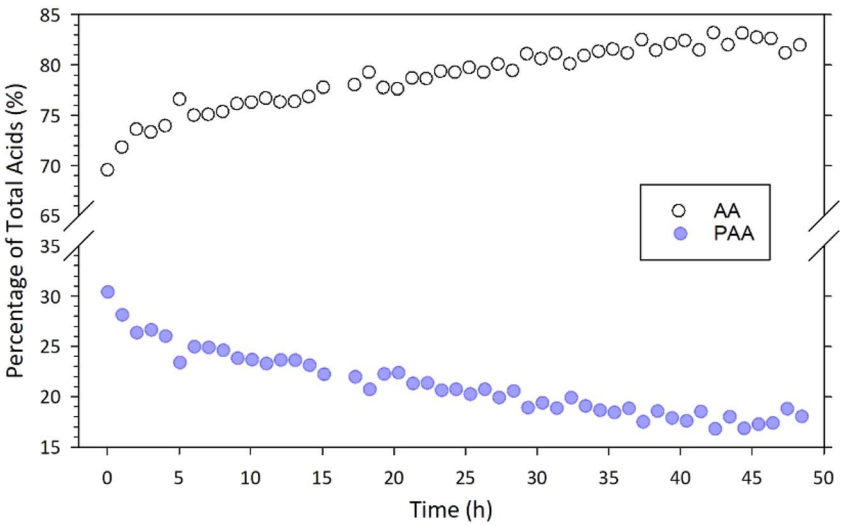

Fig. 3 A representative plot of the AA and PAA calculated as percentage of total acids in the gas phase *versus* time. Over time, the percentage of the total acids in the gas phase that was attributable to AA increased relative to the percentage of PAA, which indicated PAA decomposition to AA occurred.

exponential decay *versus* time in PVF bags however, when the PVF bags were heated (to 57 °C after 48 h storage), AA was recoverable at near 90%, which indicated that the AA losses were due to adsorption.[56] We must consider that the adsorptive process of AA also occurred for PAA, in addition to PAA decomposition.

The relative abundance of the unique products ion counts from the reaction of reagent ion NO^+ with PAA and AA has been used by Španěl *et al.* to calculate the relative percentages of each compound in the headspace from a 40% PAA solution.[50] A representative example of the sum of ions *m*/*z* 46+ and *m*/*z* 43+ for PAA and *m*/*z* 90+ and 108+ for AA, divided by the respective reaction rates for NO+ (ESI in Table S2 and eqn (S1) and (S2)†) from our experiments is shown in Fig. 3. The data in Fig. 3 was a calculation of the percentage of the total acid signal attributable to AA and PAA *versus* time from measurements of PAA in the PVF sample bag by the SIFT-MS. The relative percentage of gas-phase PAA decreasing, and AA increasing could be the result of greater surface adsorption of PAA compared to AA, though the decrease in PAA is more likely the result of PAA decomposing into AA.

Temperature dependence of the decay rate of gas-phase PAA concentration

The decay rate of gas-phase PAA concentration was measured at 10 °C, 20 °C and 30 °C for 24 hours. Fig. 4 shows the half-life of gas-phase PAA plotted as a function of temperature. The relationship between decay rate and temperature were similar for both the impinger and SIFT-MS (*m*/*z* 77+) measurements when fitted to a logarithmic function. The PAA half-life in hours (*h*) *versus* temperature was fit to a logarithmic function as measured by impinger (13) and by SIFT-MS (14).

$$h = -23.48 \ln(^\circ\mathrm{C}) + 98.77 \quad (13)$$

$$h = -23.12 \ln(^\circ\mathrm{C}) + 96.74 \quad (14)$$

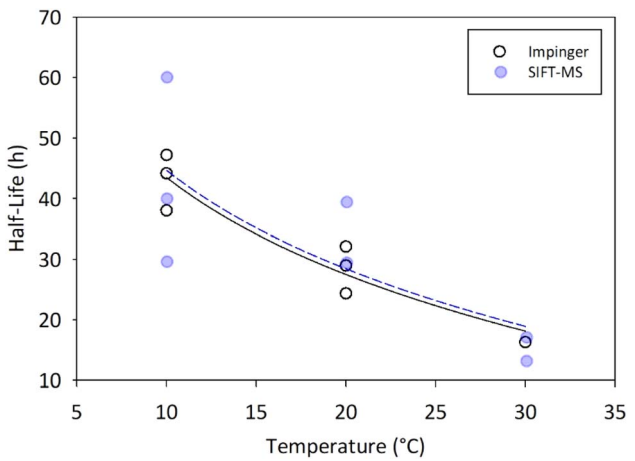

Fig. 4 Half-life of PAA in a PVF bag, determined by impinger (black, solid) and SIFT-MS (blue, dashed) measurements ($n = 3$ at 10 and 20 °C, $n = 2$ at 30 °C) *versus* temperature with logarithmic functions fitted to the data.

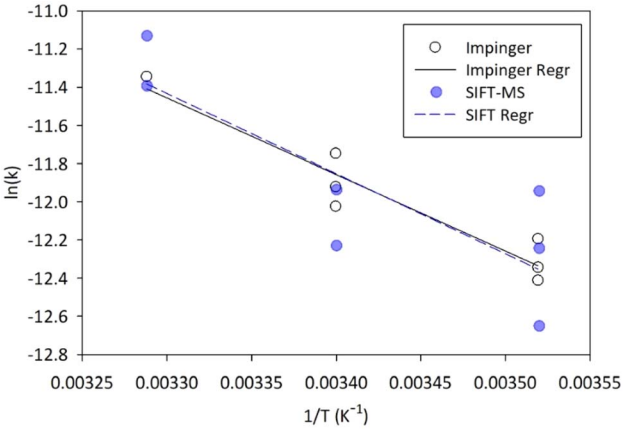

Fig. 5 Arrhenius plot of the natural log of the decay constant (*k*) of PAA *versus* the inverse of the temperature (K^{-1}) with linear regression for the impinger (black, solid line) and the SIFT-MS (blue, dashed line) data.

The data in Fig. 4 were put in the form of an Arrhenius plot, in Fig. 5, where the logarithm of the decay constant (*k*) *versus* the inverse of the temperature (K) was plotted with linear least-squares fitting to the impinger measurements resulted in (15) and SIFT-MS measurements in (16).

$$\ln(k) = (-4011 \pm 563)\cdot \mathrm{K}^{-1} + (1.78 \pm 1.94) \quad (15)$$

$$\ln(k) = (-4202 \pm 1215)\cdot \mathrm{K}^{-1} + (2.44 \pm 4.16) \quad (16)$$

From the plot in Fig. 5, the E_a for gas-phase PAA was found to be 33.4 kJ mol^{-1} for the impinger measurements and 34.9 kJ mol^{-1} for the SIFT-MS, which were averaged to 34.2 ± 1.1 kJ mol^{-1} (8.2 ± 0.3 kcal mol^{-1}). This was about half of the E_a found for the hydrolysis in aqueous conditions of 60–66 kJ mol^{-1} by Kunigk *et al.* and Zhao *et al.*[40,57,58] and a third of the 99.6 kJ mol^{-1} (23.8 kcal mol^{-1}) found by Rucker and Cates[48] in a 7.1 pH bleach solution. The E_a of hydrolysis was significantly lower than the E_a for pyrolytic decomposition of gas-phase PAA (126 to 142 kJ mol^{-1}) reported by Schmidt and Sehon.[34] In contrast to the data referenced above, the smaller E_a determined herein indicates that there was a lower energy barrier to the decay of gas-phase PAA concentrations in our system.[59]

There are numerous phenomena which are affected by temperature changes that can influence the slope of the Arrhenius plot.[60] The van't Hoff equation (from which the Arrhenius equation was based) describes the relationship between the observed equilibrium coefficients and the entropy and enthalpy of a system in equilibrium.[61,62] The observed activation energy (E_o) of reactions at a surface can be related to the true E_a for a reaction in eqn (17).[63]

$$E_o = E_a - Q_A + Q_B \quad (17)$$

where Q_A and Q_B are the heats of adsorption to a surface for a reactant A and product B, respectively.

PAA decomposition at a surface is very likely to be influenced by the presence of a reaction product such as AA. Additionally, the gas-surface concentration equilibrium affects the reaction rate at the surface. In a liquid environment, there exists a dynamic equilibrium where AA and H_2O_2 can recombine to form PAA in a reversible reaction. However, this reverse process is considerably less probable in the gas phase or at a gas-surface interface. The role of the PVF surface in the observations reported herein is not definitively known. The internal hydrogen bonding in PAA for conformers of rotation around the O–O bond was ~20 kJ mol^{-1} as calculated by Harza *et al.*[64] If PAA surface adsorption is contingent on disrupting the internal hydrogen bonding, then 20 kJ mol^{-1} may be indicative of an energy maximum that has to be overcome for surface adsorption.

In general, decreasing temperatures favor adsorption of gases to surfaces, and slow the rates of decomposition reactions. Conversely, temperature increases reduce surface adsorption of gases (gas-surface partitioning), increases diffusion, and increase reaction rates. In the data herein, the half-life of gas-phase PAA decreased at higher temperatures (in Fig. 4), indicating that reversible surface adsorption was not the limiting mechanism by which gas-phase PAA concentrations decreased. This leaves irreversible surface adsorption (meditated by diffusion) and decompositions reactions as possible limiting factors for the decay of gas-phase PAA concentrations.

Given the relatively long time frames observed herein for the half-life of gas-phase PAA concentration, we have to interpret the rapid 22 minutes, and 83 minutes room temperature half-lives of gas-phase PAA concentrations, reported by Ancker and Zetterberg, and Hines *et al.*, as having been largely influenced by interactions of PAA with the container surface.[29,42,43] The E_a of 34 kJ mol^{-1} we observed for temperature dependent decay of gas-phase PAA concentration was lower than other estimates of E_a of gas-phase PAA decomposition, which indicated that other factors, most likely diffusion to and interactions at the PVF surface, affected the results. Through whichever mechanisms the decreases in gas-phase PAA concentration occurred, it was relatively slow and exhibited temperature dependence if the half-life.

We attempted to investigate the humidity dependence of the half-life of gas-phase PAA in the PVF bag. The results and a discussion of the difficultly of drawing a conclusion from the half-life data collected over a range of humidities have been included in ESI (Fig.s S3 and S4).† The measured half-life of PAA did not show a discernible correlation to the initial humidities of the generated PAA atmospheres. The diffusivity of water through PVF made it so that we could not conclude that the water content of the generated atmospheres remained in the PVF bag.

Conclusions

Gas-phase PAA concentrations exhibited exponential decay *versus* time consistent with first order kinetics. The rate of change of gas-phase PAA concentrations observed with both SIFT-MS (H_3O^+ *m*/*z* 77+) and impinger measurements were in good agreement. The half-life of gas-phase PAA concentration in an isolated environment of a PVF bag was shown to vary with temperature, which ranged from 18 hours at 30 °C to 45 hours at 10 °C. The decay constant fit to an Arrhenius plot was used to calculate an E_a of 34.2 kJ mol^{-1}.

This E_a was notably lower than the E_a reported by other researchers for PAA decomposition in liquid or gas phase. It is likely that the observed kinetics were composed of several decay pathways including reactions and surface adsorption rather than a rate constant of a single reaction mechanism.

Both PAA and AA concentrations in the gas-phase decreased with time. The experiments within were not able to distinguish between contributions of surface adsorption *versus* decomposition that led to the deceases in gas-phase PAA. The change in the ratio of AA to PAA increased with time indicating that PAA decomposition was occurring.

The half-lives of gas-phase PAA concentrations were relatively long. The slow rate of PAA decay in these experiments led us to surmise that during disinfection processes in an indoor environment, air exchanges and interactions at the surface would have a greater influence on decreasing the gas-phase PAA concentration than the rate of gas-phase decomposition.

Disclaimer

The findings and conclusions in this report are those of the authors and do not necessarily represent the official position of the National Institute for Occupational Safety and Health, Centers for Disease Control and Prevention. Mention of any company or product does not constitute endorsement by the National Institute for Occupational Safety and Health, Centers for Disease Control and Prevention.

This activity was reviewed by CDC and was conducted consistent with applicable federal law and CDC policy. §See *e.g.*, 45 C.F.R. part 46; 21 C.F.R. part 56; 42 U.S.C. §241(d), 5 U.S.C. §552a, 44 U.S.C. §3501 et seq.

Data availability

Datasets are available online at the CDC data repository at **https://www.data.cdc.gov/**.

Author contributions

Amos Doepke contributed to the project conceptualization, data curation, formal analysis, investigation, methodology, and writing the original draft. Robert P. Streicher contributed to the project conceptualization and editing of the manuscript. Angela L. Stastny contributed to the project conceptualization and editing of the manuscript.

Conflicts of interest

There are no conflicts to declare.

Acknowledgements

Generative artificial intelligence model (ChaptGPT 4.o) was used to improve grammar, clarity, and readability of certain sections of the manuscript drafted by authors. The AI model was not used for content creation or text generation.

References

1 Q. Q. Wu, L. B. Huang, H. Liang, Y. Zhao, D. Huang and Z. M. Chen, Heterogeneous reaction of peroxyacetic acid and hydrogen peroxide on ambient aerosol particles under dry and humid conditions: kinetics, mechanism and implications, *Atmos. Chem. Phys.*, 2015, **15**, 6851–6866.

2 M. Berasategui, D. Amedro, L. Vereecken, J. Lelieveld and J. N. Crowley, Reaction between $CH_3C(O)OOH$ (peracetic acid) and OH in the gas phase: a combined experimental and theoretical study of the kinetics and mechanism, *Atmos. Chem. Phys.*, 2020, **20**, 13541–13555.

3 H. A. Rypkema and J. S. Francisco, Atmospheric Oxidation of Peroxyacetic Acid, *J. Phys. Chem. A*, 2013, **117**, 14151–14162.

4 X. Zhang, Z. M. Chen, S. Z. He, W. Hua, Y. Zhao and J. L. Li, Peroxyacetic acid in urban and rural atmosphere: concentration, feedback on PAN-NO cycle and implication on radical chemistry, *Atmos. Chem. Phys.*, 2010, **10**, 737–748.

5 C.-L. Xie, H. Yang and B. Long, Reaction between peracetic acid and carbonyl oxide: Quantitative kinetics and insight into implications in the atmosphere, *Atmos. Environ.*, 2025, **341**, 120928.

6 S. Wang, E. C. Apel, R. S. Hornbrook, A. Hills, L. K. Emmons, S. Tilmes, J. F. Lamarque, J. L. Jimenez, P. Campuzano-Jost, B. A. Nault, J. D. Crounse, P. O. Wennberg, T. B. Ryerson, C. R. Thompson, J. Peischl, F. Moore, D. Nance, B. Hall, J. Elkins, D. Tanner, L. Gregory Huey, S. R. Hall, K. Ullmann, J. J. Orlando, G. S. Tyndall, F. M. Flocke, E. Ray, T. F. Hanisco, G. M. Wolfe, J. St Clair, R. Commane, B. Daube, B. Barletta, D. R. Blake, B. Weinzierl, M. Dollner, A. Conley, F. Vitt, S. C. Wofsy and D. D. Riemer, Atmospheric Acetaldehyde: Importance of Air-Sea Exchange and a Missing Source in the Remote Troposphere, *Geophys. Res. Lett.*, 2019, **46**, 5601–5613.

7 J. N. Crowley, N. Pouvesle, G. J. Phillips, R. Axinte, H. Fischer, T. Petäjä, A. Nölscher, J. Williams, K. Hens, H. Harder, M. Martinez-Harder, A. Novelli, D. Kubistin, B. Bohn and J. Lelieveld, Insights into HO_x and RO_x chemistry in the boreal forest *via* measurement of peroxyacetic acid, peroxyacetic nitric anhydride (PAN) and hydrogen peroxide, *Atmos. Chem. Phys.*, 2018, **18**, 13457–13479.

8 S. Z. He, Z. M. Chen, X. Zhang, Y. Zhao, D. M. Huang, J. N. Zhao, T. Zhu, M. Hu and L. M. Zeng, Measurement of atmospheric hydrogen peroxide and organic peroxides in Beijing before and during the 2008 Olympic Games: Chemical and physical factors influencing their concentrations, *J. Geophys. Res.:Atmos.*, 2010, **115**, D17307.

9 Z. Yuan, Y. Ni and A. R. P. Van Heiningen, Kinetics of peracetic acid decomposition: Part I: Spontaneous decomposition at typical pulp bleaching conditions, *Can. J. Chem. Eng.*, 1997, **75**, 37–41.

10 N. Pechacek, M. Osorio, J. Caudill and B. Peterson, Evaluation of the toxicity data for peracetic acid in deriving occupational exposure limits: a minireview, *Toxicol. Lett.*, 2015, **233**, 45–57.

11 B. H. Blackley, M. A. Virji, R. R. Harvey, J. Cox-Ganser and R. J. Nett, Evaluation of exposure to a hydrogen peroxide, peracetic acid, and acetic acid containing cleaning and disinfection product and symptoms in hospital employees, In Report No. 2017-0114-3357, Centers for Disease Control and Prevention, National Institute for Occupational Safety and Health, 2019.

12 O. Cerne, K. Ancker and P. Palokangas, *(Swedish) Working Environment and Environmental Effects of the Pulp Industry's Environmental Adaptation: Peracetic Acid as a Bleaching Chemical and a Feasibility Study of Closing Process Water Streams*, Swedish Environmental Research Institute, Stockholm, 1999.

13 R. J. Yokelson, J. D. Crounse, P. F. DeCarlo, T. Karl, S. Urbanski, E. Atlas, T. Campos, Y. Shinozuka, V. Kapustin, A. D. Clarke, A. Weinheimer, D. J. Knapp, D. D. Montzka, J. Holloway, P. Weibring, F. Flocke, W. Zheng, D. Toohey, P. O. Wennberg, C. Wiedinmyer, L. Mauldin, A. Fried, D. Richter, J. Walega, J. L. Jimenez, K. Adachi, P. R. Buseck, S. R. Hall and R. Shetter, Emissions from biomass burning in the Yucatan, *Atmos. Chem. Phys.*, 2009, **9**, 5785–5812.

14 G. I. Walters, P. S. Burge, V. C. Moore, M. O. Thomas and A. S. Robertson, Occupational asthma caused by peracetic acid-hydrogen peroxide mixture, *Occup. Med.*, 2019, **69**, 294–297.

15 J. Wang, J. Xu, J. Kim and C. H. Huang, Mechanistic Insight for Disinfection Byproduct Formation Potential of Peracetic Acid and Performic Acid in Halide-Containing Water, *Environ. Sci. Technol.*, 2023, **57**, 18898–18908.

16 S. Mondal, E. Mackey and R. Hofmann, Peracetic acid to reduce disinfection by-product formation in drinking water, *Environ. Sci.:Water Res. Technol.*, 2024, **10**, 1499–1505.

17 United States Enviromental Protection Agency (EPA), *ChemView*, Chemical Data Reporting 2012-2019, **https://www.chemview.epa.gov/chemview**.

18 B. H. Blackley, R. J. Nett, J. M. Cox-Ganser, R. R. Harvey and M. A. Virji, Eye and airway symptoms in hospital staff exposed to a product containing hydrogen peroxide, peracetic acid, and acetic acid, *Am. J. Ind. Med.*, 2023, **66**, 655–669.

19 I. Fong, S. Y. Chew and K. L. Tan, A 27-Year-Old Man With Persistent Breathlessness After an Inhalational Injury, *Chest*, 2021, **159**, e197–e201.

20 A. L. Stastny, A. Doepke and R. P. Streicher, A field-portable colorimetric method for the measurement of peracetic acid vapors: a comparison of glass and plastic impingers, *J. Occup. Environ. Hyg.*, 2022, **19**, 469–477.

21 American Conference of Governmental Industrial Hygienists (ACGIH®), *PERACETIC ACID: TLV® Recommendation*, 2014.

22 National Center for Biotechnology Information*PubChem Compound Summary for CID 6585, Peracetic Acid*National Library of Medicine (US), **https://pubchem.ncbi.nlm.nih.gov/compound/Peracetic-Acid** (accessed Sept. 9, 2024).
23 X. Ding, J. Jiang, A. D. Shah and N. Jung, Peracetic acid emissions and exposures during building disinfection events, *Building and Environment*, 2025, **269**.
24 M. Pacenti, S. Dugheri, P. Boccalon, G. Arcangeli, P. Dolara and V. Cupelli, Air monitoring and assessment of occupational exposure to peracetic acid in a hospital environment, *Ind. Health.*, 2010, **48**, 217–221.
25 N. C. Burton and J. Gibbins, *Evaluation of Peracetic Acid Exposure Among Federal Poultry Inspectors*, 2017.
26 N. C. Burton and J. Gibbins, *Assessment of Peracetic Acid Exposure Among Federal Poultry Inspectors*, 2016.
27 B. D. Kerger, A. E. Loccisano and P. Dalton, in *Human and Ecological Risk Assessment*, 2024, pp. 671–716, doi: DOI: **10.1002/9781119742975.ch18**.
28 E. Kruszewska, H. Grzes, P. Czupryna, S. Pancewicz, M. Groth, M. Wondim and A. Moniuszko-Malinowska, Fogging With Peracetic Acid in Schools and Kindergartens, *Front Public Health*, 2021, **9**, 697917.
29 R. Hines, C. Y. Chen, M. Nicas and G. Ramachandran, Estimating the time-varying emission rate of peracetic acid, *Ann. Work Exposures Health*, 2025, **69**, 297–309.
30 I. DuPont de Nemours, *DuPont Technical Bulletin - Chemical Resistance of Tedlar® PVF Films*, 2021.
31 L. Ernstgard, B. Sjogren and G. Johanson, Acute effects of exposure to vapors of hydrogen peroxide in humans, *Toxicol. Lett.*, 2012, **212**, 222–227.
32 L. J. McGarvey and C. V. Shorten, The effects of adsorption on the reusability of Tedlar air sampling bags, *AIHAJ*, 2000, **61**, 375–380.
33 N. Musakka, T. Salmi, J. WärnÅ, J. Ahlkvist and M. Piironen, Modelling of organic liquid-phase decomposition reactions through gas-phase product analysis: Model systems and peracetic acid, *Chem. Eng. Sci.*, 2006, **61**, 6918–6928.
34 C. Schmidt and A. H. Sehon, The Thermal Decomposition of Peracetic Acid in the Vapor Phase, *Can. J. Chem.*, 1963, **41**, 1819–1825.
35 X. Zhao, K. Cheng, J. Hao and D. Liu, Preparation of peracetic acid from hydrogen peroxide, part II: Kinetics for spontaneous decomposition of peracetic acid in the liquid phase, *J. Mol. Catal. A:Chem.*, 2008, **284**, 58–68.
36 E. Koubek, M. L. Haggett, C. J. Battaglia, K. M. Ibne-Rasa, H. Y. Pyun and J. O. Edwards, Kinetics and Mechanism of the Spontaneous Decompositions of Some Peroxoacids, Hydrogen Peroxide and t-Butyl Hydroperoxide, *J. Am. Chem. Soc.*, 2002, **85**, 2263–2268.
37 Y.-W. Wang, M.-S. Liao and C.-M. Shu, Thermal hazards of a green antimicrobial peracetic acid combining DSC calorimeter with thermal analysis equations, *J. Therm. Anal. Calorim.*, 2015, **119**, 2257–2267.
38 B. K. Keller, M. D. Wojcik and T. R. Fletcher, A directly-dissociative stepwise reaction mechanism for gas-phase peroxyacetic acid, *J. Photochem. Photobiol., A*, 2008, **195**, 10–22.
39 H. Wu, Y. Wang, H. Li, L. Huang, D. Huang, H. Shen, Y. Xing and Z. Chen, The OH-initiated oxidation of atmospheric peroxyacetic acid: Experimental and model studies, *Atmos. Environ.*, 2017, **164**, 61–70.
40 L. Kunigk, D. R. Gomes, F. Forte, K. P. Vidal, L. F. Gomes and P. F. Sousa, The influence of temperature on the decomposition kinetics of peracetic acid in solutions, *Braz. J. Chem. Eng.*, 2001, **18**, 217–220.
41 F. W. Evans and A. H. Sehon, The Thermal Decomposition of Peracetic Acid in Aromatic Solvents, *Can. J. Chem.*, 1963, **41**, 1826–1831.
42 European Centre for Ecotoxicology and Toxicology of Chemicals, *ECETOC JACC No.40. Peracetic Acid (CAS No. 79-21-0) and its Equilibrium Solutions*, Brussels, 2001.
43 K. Ancker and L. Zetterberg, *Measurement of peracetic acid at Eka Chemicals AB Bohus*, Unpublished Report No. A97329, IVL, Stockholm, Sweden, Eka Chemicals, Bohus, Sweden, 1997.
44 K. Ancker, *LP-FTIR med en makro-kyvett för mätning i arbetsmiljön.*, Institutet för Vatten- och Luftvårdsforskning, Stockholm, Sweden, IVL Rapport B1284, 1998.
45 Z. A. Piskulich, O. O. Mesele and W. H. Thompson, Activation Energies and Beyond, *J. Phys. Chem. A*, 2019, **123**, 7185–7194.
46 R. Bianchini, L. Calucci, C. Lubello and C. Pinzino, Intermediate free radicals in the oxidation of wastewaters, *Res. Chem. Intermed.*, 2002, **28**, 247–256.
47 R. C. Weast, ed., *Handbook of Chemistry and Physics*, CRC Press, Boca Raton, Florida, 1982.
48 J. W. Rucker and D. M. Cates, 2,2î-Bipyridine Catalyzed Bleaching of Cotton Fibers with Peracetic Acid, *Text. Res. J.*, 2016, **58**, 148–160.
49 V. S. Langford, K. Dryahina and P. Spanel, Robust Automated SIFT-MS Quantitation of Volatile Compounds in Air Using a Multicomponent Gas Standard, *J. Am. Soc. Mass Spectrom.*, 2023, **34**, 2630–2645.
50 P. Španěl, A. M. Diskin, T. Wang and D. Smith, A SIFT study of the reactions of H3O+, NO+ and O2+ with hydrogen peroxide and peroxyacetic acid, *Int. J. Mass Spectrom.*, 2003, **228**, 269–283.
51 P. Španěl and D. Smith, SIFT studies of the reactions of H3O+, NO+ and O+2 with a series of volatile carboxylic acids and esters, *Int. J. Mass Spectrom. Ion Processes*, 1998, **172**, 137–147.
52 A. Doepke, A. L. Stastny and R. P. Streicher, Controlled generation of peracetic acid atmospheres for the evaluation of chemical samplers, *Anal. Methods*, 2021, **13**, 3799–3805.
53 K. B. Haase, W. C. Keene, A. A. P. Pszenny, H. R. Mayne, R. W. Talbot and B. C. Sive, Calibration and intercomparison of acetic acid measurements using proton-transfer-reaction mass spectrometry (PTR-MS), *Atmos. Meas. Tech.*, 2012, **5**, 2739–2750.
54 C. Cavallotti, M. Pelucchi and A. Frassoldati, Analysis of acetic acid gas phase reactivity: Rate constant estimation and kinetic simulations, *Proc. Combust. Inst.*, 2019, **37**, 539–546.

55 M. Fido, S. Hersberger, A. T. Guntner, R. Zenobi and S. Giannoukos, Systematic study of polymer gas sampling bags for offline analysis of exhaled breath, *J. Breath Res.*, 2024, **18**(4), DOI: **10.1088/1752-7163/ad6a31**.

56 P. L. Kasper, A. Oxbol, M. J. Hansen and A. Feilberg, Mechanisms of Loss of Agricultural Odorous Compounds in Sample Bags of Nalophan, Tedlar, and PTFE, *J. Environ. Qual.*, 2018, **47**, 246–253.

57 L. Kunigk, S. M. Silva and C. H. Jurkiewicz, The influence of temperature and organic matter on the decomposition kinetics of peracetic acid in aqueous solutions, *Lat. Am. Appl. Res.*, 2012, **43**, 291–297.

58 X. Zhao, T. Zhang, Y. Zhou and D. Liu, Preparation of peracetic acid from hydrogen peroxide: Part I: Kinetics for peracetic acid synthesis and hydrolysis, *J. Mol. Catal. A: Chem.*, 2007, **271**, 246–252.

59 I. W. Smith, The temperature-dependence of elementary reaction rates: beyond Arrhenius, *Chem. Soc. Rev.*, 2008, **37**, 812–826.

60 P. D. Pacey and J. H. Purnell, Arrhenius parameters of the reaction $CH_3\cdot + C_2H_6 \rightarrow CH_4 + C_2H_5\cdot$, *J. Chem. Soc., Faraday Trans.*, 1972, **68**.

61 H. Eyring, The Activated Complex and the Absolute Rate of Chemical Reactions, *Chem. Rev.*, 1935, **17**, 65–77.

62 R. R. Krug, W. G. Hunter and R. A. Grieger, Enthalpy-entropy compensation. 1. Some fundamental statistical problems associated with the analysis of van't Hoff and Arrhenius data, *J. Phys. Chem.*, 1976, **80**, 2335–2341.

63 H. S. Taylor, The activation energy of adsorption processes, *J. Am. Chem. Soc.*, 1931, **53**, 578–597.

64 M. K. Hazra, X. Kuang and A. Sinha, Influence of intramolecular hydrogen bonding on OH-stretching overtone intensities and band positions in peroxyacetic acid, *J. Phys. Chem. A*, 2012, **116**, 5784–5795.